Evaluation of 3D Printing Technology for Corrugated Horn Antenna Manufacturing

Emmanuel Decrossas, Theodore Reck, Choonsup Lee, Cecile Jung-Kubiak, Imran Mehdi and Goutam Chattopadhyay
Jet Propulsion Laboratory,
California Institute of Technology
Pasadena, CA, 91109
Emmanuel.Decrossas@jpl.nasa.gov

***Abstract*— We report on the performance of waveguide components at W-band manufactured with 3-D printing technology. The precision and surface roughness of the various techniques are studied to determine the applicability of millimeter-wave components. The best waveguide attenuation measured of 0.014 dB/mm is still three times higher than for metal WR-10 waveguides. Full-wave simulations and surface roughness analysis show that performance can be improved by changing the orientation of the parts in the printer. The performance of a multi-flare angle and corrugated horn antennas is evaluated.**

Keywords — 3-D printing, corrugated horn, metal sintering, horn, surface roughness, waveguide attenuation, W-band, WR-10 waveguide.

I. Introduction

3-D printing is an emerging technology enabling the fabrication of complex three dimensional objects directly from a computer-aided design (CAD) digital model [1]. It has been successfully applied for both prototyping and distributed manufacturing in jewelry, biotech, industrial design, and other areas [1-3]. The additive process used in 3-D printing technology differs from traditional computer numerical control (CNC) metal machining where the metal is removed from bulk material. Building of terahertz components using traditional metal-machining techniques is expensive, time consuming, and a serial process where each piece needs to be machined independently. Therefore, for multi-pixel receivers [4] where many components are needed to be assembled for working instruments, it becomes prohibitively expensive. This paper highlights the advantages of this low-cost and highly efficient process to fabricate a lot of corrugated horns at lower cost. Recently, progress in 3-D printing has enabled application of this technique to Ku-band (12-15 GHz) horn antenna [5] using electron beam melting (EBM). Garcia *et al.* found that this Ku-Band horn had a rms surface roughness of 40 µm, degrading its performance by 1 dB [5].

The more commonly available commercial 3-D printing technique developed by Stratsys is the fused deposition modeling (FDM) process, where melted thermoplastic is extruded in small beads which harden immediately. Many patterned layers are applied to form the desired three dimensional objects. The second printing method, called Polyjet, consists of layers of liquid photopolymer cured with ultraviolet (UV) light. The Polyjet-based 3-D printer offers the highest resolution commercially available of 600x600x1600 DPI producing 16 µm thick layers with an accuracy of 100 µm.

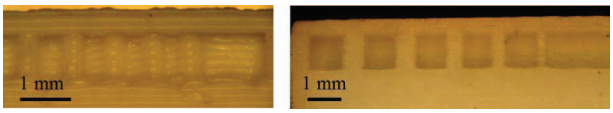

Fig. 1. Minimum feature size test features used to estimate the resolution of the 3-D printing technology using FDM technology (left) and using Polyjet method (right).

Fig. 1 shows a minimum line width test feature varying from 500 µm to 100 µm fabricated in both FDM and PolyJet, and compares the resolution of these two processes. Clearly, the FDM process doesn't have the resolution required for devices at W-band. Due to FDM's poor resolution, only Polyjet components were tested in this study.

An overview of different fabrication techniques and their performance at W-band and above is presented in this paper including 3-D printing polymer metallized with sputtered and plated gold and direct metal laser sintered (DMLS). To the best of our knowledge, this is the first time 3-D printing technology is used to fabricate and evaluate waveguide components at W-band frequencies and above.

The testing structure as shown in Fig. 2 consists of straight 1 cm long, hollow rectangular waveguides varying from WR-10(2.54x1.27 mm) to WR-1.5(0.381x0.19 mm). Corresponding E-plane split waveguide sections are also included on the edges as waveguide devices often require joining two metal blocks together to form the hollow waveguide structure.

II. Fabrication and Measurements

A. 3-D printing metalized polymer

3-D printing Polyjet matte surface finish benchmark components as seen in Fig. 2 were metallized using gold sputtering and gold plating. First, a gold layer 2 µm thick was

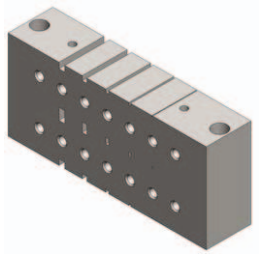

Fig. 2. Benchmark component used to characterize the various processes' ability to produce straight waveguide sections varying from WR-10 (2.54x1.27 mm) to WR-1.5 (0.381x0.19 mm).

sputtered with a 300 Å thin adhesion layer of titanium. Although, the metal delaminated from the surface of the polymer, the internal sidewalls of the fabricated hollow rectangular WR-10 waveguide seem to maintain their metallization.

The scattering parameters are measured with an HP8510C network analyzer with WR-10 extenders. The estimated waveguide attenuation for the gold sputtered Polyjet hollow rectangular waveguide are found to be 1.5-2 dB/mm. This very large waveguide loss is attributed to a combination of the high surface roughness and the sidewalls not well metallized due to the gold delamination.

The second metallization technique applied is gold plating. First, a thin layer of Nickel is first electrolessly deposited on the 3-D printing polymer, and then the part is successively plated in electrolytic solutions of copper, nickel and gold. The total metallization thickness varies from 2 µm to 7 µm.

The measured return loss above 10 dB is mainly due to small area in the hollow waveguide without metallization and partially to misalignment between the waveguides and mismatch cross section between the WR-10 waveguide (2.54x1.27 mm) and our device under test (DUT) (2.58x1.24 mm) as confirmed by our simulated model in high frequency structural simulator (HFSS). The waveguide attenuation (WA) is computed from the measured scattering parameters using the following formula to isolate the attenuated power or fractional power loss in the waveguide taking into account the reflected input lost power:

$$P_{L,\mathrm{dB}} = 10\log_{10}(|S_{11}|^2 + |S_{21}|^2) \qquad (1)$$

The estimated WA calculated with (1), considering the 10 mm long hollow rectangular waveguide, are 0.1-0.36 dB/mm. Again, this is attributed to the roughness of the side walls and reduced metallization along the waveguide sidewalls. For comparison, the measured waveguide loss with the network analyzer through a 50.12 mm long metal WR-10 rectangular waveguide is estimated to be 0.004-0.008 dB/mm.

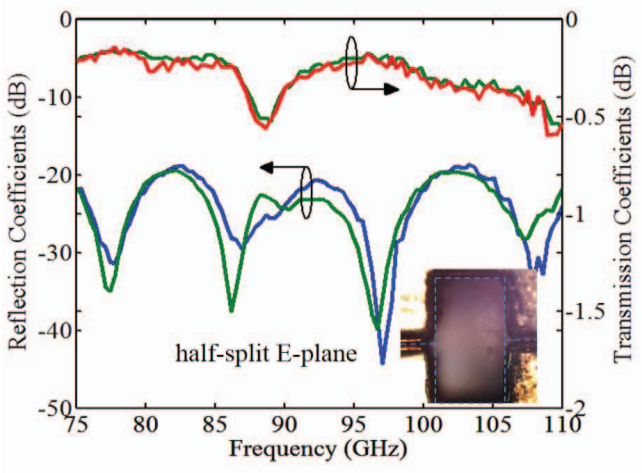

Fig. 3. Measured reflection and transmission coefficients of the gold plated Polyjet E-plane half-split WR-10 rectangular waveguide as shown in the inset.

By fitting the measured transmission coefficients into HFSS, it is found that the effective conductivity (σ) is about 3×10^7 S/m after applying a 0.3 µm rms surface roughness, following the Groiss model [6] that is consistent with [7-8]. Besides the fabrication tolerances, the main limiting factors are surface roughness and metallization of the polymer. The metallization coverage can be improved by splitting the waveguide in half similar to the ones used in traditional metal machining or by reducing the waveguide aspect ratio (ratio between the cross section of the waveguide and the length of the waveguide).

Measurements of the gold plated Polyjet split in half following the E-plane is presented in Fig. 3. Both halves of the waveguide are plated and combined to form the complete hollow waveguide. The metallization of the surface is enhanced as the flux of the electrolytic solutions during the plating process is higher over a surface than through the hollow waveguide. From the measurement presented in Fig. 3, the estimated waveguide attenuation is 0.03-0.12 dB/mm at W-band using (1).

B. 3-D metal printing

The same benchmark part shown in Fig. 2 is fabricated using an additional 3-D printing method called direct metal laser sintered (DMLS) technique. This process consists of fusing metal powder into a solid part by melting it locally using a focused laser beam, similar to the technique employed in [5]. While this technique has the advantage of not needing additional metallization, the fabrication precision is lower than the Polyjet process. In fact, the cross section of the hollow rectangular waveguide is measured to be 2.43x1.40 mm, which is off by at least 100 µm compared to our original design. The reflection coefficients are below -12 dB over the W-band indicating a moderate match and the extracted waveguide attenuation of 0.02-0.7 dB/mm is still 10 times higher than metallic WR-10 waveguides, again caused by high surface roughness.

C. Surface roughness analysis

The rms surface roughness of the 3-D printed waveguide sections is characterized with a Dektak stylus profilometer. Fig. 4 shows a representative scan of the bottom surface of the waveguides for the 3-D printing Polyjet without metal, the gold plated 3-D printing Polyjet, and the aluminum DMLS. It should be noted that metal plating the Polyjet parts significantly smooth the surface of the waveguide. Several models have been developed to estimate the surface resistance based on the roughness of the surface finish. Those empirical formulae such as Groiss [6] and Hammerstad [9] are usually applied to relatively smooth surfaces where the surface roughness is in the same order or less than the skin depth. Another method consists of adjusting the conductivity value in the simulation to fit the experimental measurements as the conductivity varies with the metal purity and the surface roughness [8]. For all the 3-D printed parts, the peak to peak surface roughness is around 25 µm as shown in Fig. 4 which makes those formulae unsuitable since the skin depth is less than half a micron at W-band. Instead, the surface roughness profile along the printing axis,

shown in Fig. 4, is integrated in a 3-D finite element model. Three printing orientations are presented in Fig. 5. This simulation illustrates that the loss can be improved by orienting the parts differently in the printer. The gold conductivity used in the model ($\sigma=5x10^6$ S/m) is adjusted by fitting the simulated data with measurements presented in Fig. 3.

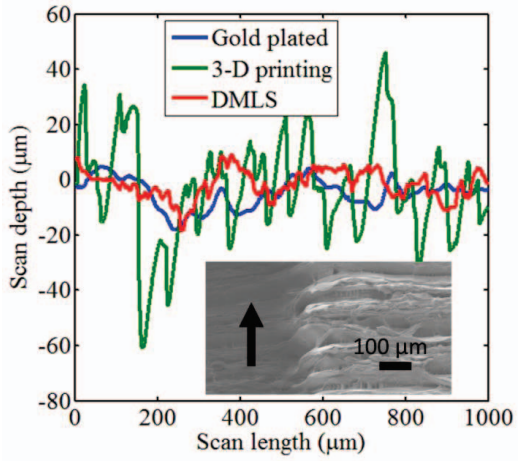

Fig. 4. Profilometer traces of a representative surface roughness at the waveguide inside sidewalls for the 3-D printing Polyjet (green), gold plated 3-D printing Polyjet (blue) and aluminum DMLS (red). The inset shows the SEM picture of the Polyjet inside sidewall surface of the hollow rectangular waveguide and the arrow the scanning direction along the printing axis.

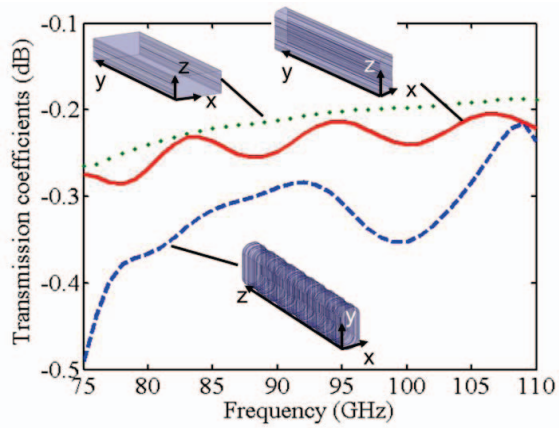

Fig. 5. Simulated transmission coefficients of 10 mm long 3-D printing waveguide using HFSS considering different printing orientation (z-axis) using the surface profile shown in Fig.4.

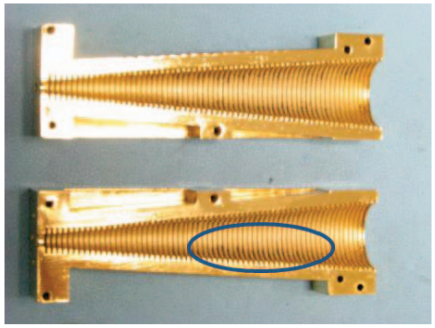

Fig. 6. Split blocks of the fabricated corrugated horn after gold plating. The circle indicates the non-metallized areas.

Furthermore, the surface roughness can be reduced by changing the orientation of the parts in the 3-D printer as illustrated by fig. 5. The results of the various components tested are summarized in Table I. The rms surface roughness is measured along the waveguide cut sidewall (wide side) using a profilometer.

TABLE I
Comparison of the 3-D printing techniques

3-D printing technique	Measured results		
	Waveguide attenuation (dB/mm)	Cost ($)	Surface quality
Sputtered polymer	1.5–2	~150	delamination of gold 25 µm surface roughness <100 µm fabrication tolerance
Plated polymer	0.1–0.36	~150	25 µm surface roughness <100 µm fabrication tolerance sidewall not well metallized
Plated polymer half-split	0.03–0.12	~150	25 µm surface roughness <100 µm fabrication tolerance
Aluminum DMLS	0.02–0.7	~2000	300 µm protuberance 30 µm surface roughness >100 µm fabrication tolerance
Metal machining	0.004–0.008	~200	~0.3 µm surface roughness from [7]

III. Corrugated Horn Antenna

A. Design and simulation

The design presented in Fig. 6 shows split blocks of the 3D printed corrugated horn after gold plating. It can be seen on the photograph that small dark areas are not metallized. So, an extra 1 µm gold layer was sputtered on top of each block to enhance the performance of the horn by reducing the ohmic losses.

The designed corrugated horn dimensions are specified in Fig.7. The grooves are 0.6 mm wide with a pitch of 1.21 mm and 0.74 mm deep. The aperture angle of the horn is 175.4 degree and the total length of the horn is 79 mm.

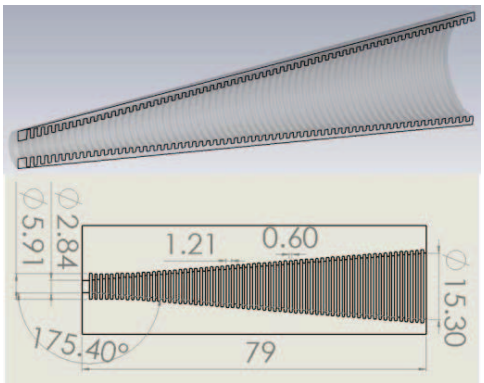

Fig. 7. As simulated corrugated horn antenna cut in half and mechanical drawing with dimensions in millimeters.

The simulations are performed using mode matching [10] and 3D EM solver CST: the results are presented in fig. 8. Again the value of the conductivity is adjusted based on the measurement (σ=3.10^7 S/m) taking into account the finite conductivity of gold and rms surface roughness of the sidewalls which lead to a simulated radiation efficiency of 99%.

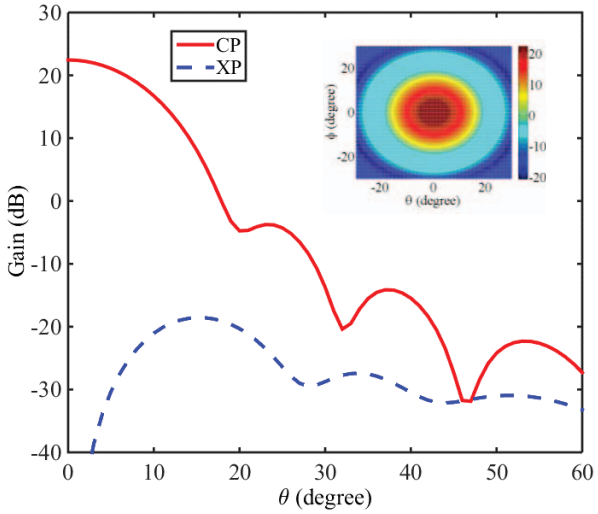

Fig. 8. Simulated Gain with CST of the corrugated horn antenna at 99 GHz. The inset shows the amplitude in azimuth and elevation.

B. Measurements

The measurements of the reflection coefficients carried out with a network analyzer via W-band extenders are presented in Fig. 9.

The difference between the measured and simulated reflection coefficients are mainly due to non-uniformity of the metallization, misalignment between the blocks, small air gap interstice between the blocks when combined due to the surface roughness and flatness of the 3D printed blocks. Furthermore, after inspecting the fabricated parts under the microscope, it is found that the groove spacing is 0.712 mm with a deviation of ±25µm and the measured width is 0.485 mm with a deviation of ±25µm. The normalized gain is measured as shown in Fig. 10.

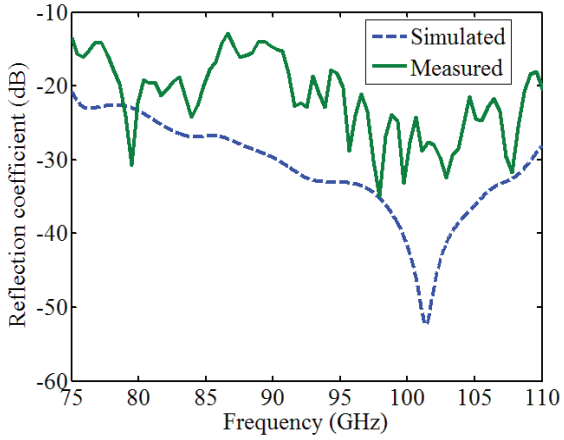

Fig. 9. Measured and simulated reflection coefficients of the corrugated horn antenna presented in fig. 6.

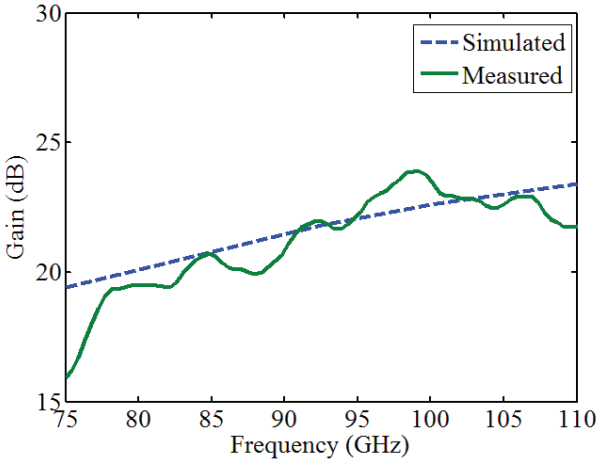

Fig. 10. Measured and simulated gain of the corrugated horn illustrated in Fig. 6 versus frequency.

Although at lower frequencies, the misalignment between the blocks and the fabrication tolerances becomes minor factors, the non-uniformity of the metallization is still an issue, as presented in [11] at Ku-band and W-band [12].

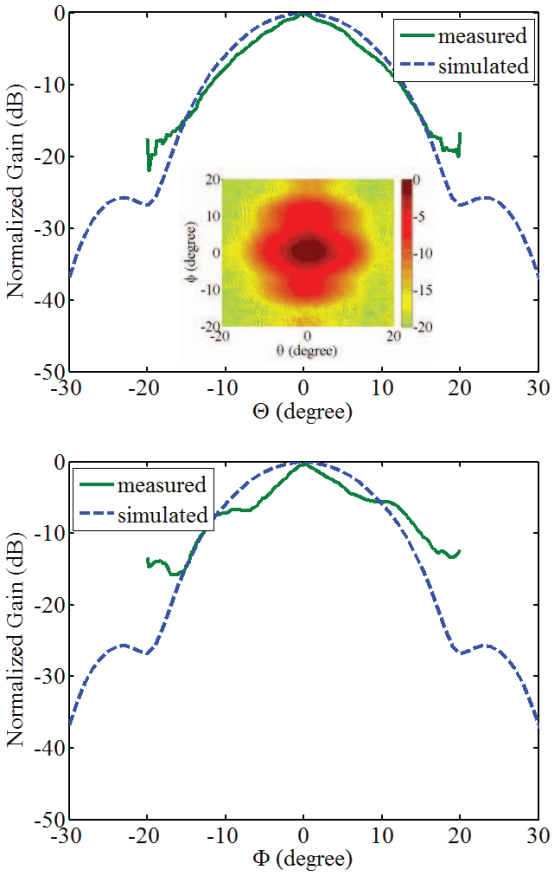

Fig. 11. Normalized measured and simulated gain functions of the azimuthal angle (top plot) and elevation angle (bottom plot). It should be noted that measured data (green solid curve) are limited by the sensitivity of the mixer/receiver explaining that over 10 degrees the response of the mixer becomes flat. The inset shows the 2D view of the measured normalized gain.

The beam pattern is measured using a W-band harmonic mixer connected to a 24 dB standard gain antenna. The measured antenna is connected to a 99 GHz synthesizer. A chopper and lock-in amplifier are used between the two horns to maximize signal-to-noise ratio and obtain accurate data. The standard gain antenna is mounted on a moving platform to measure the elevation and azimuthal pattern over a 40 degrees angle aperture.

CONCLUSION

Although the fabrication tolerance of the Polyjet process seems capable of defining W-band microwave waveguides, surface roughness is a limiting factor. By splitting the block along the E-plane, we have been able to reduce loss due to the better metallized surface. However, the surface roughness is still high and produces waveguide attenuation three to five times higher than for traditional CNC metal machining. Finite-element simulations show that the results can be improved by carefully choosing the orientation of the printing parts in the printer. Hopefully, with further refinement of these techniques, 3-D printing could be an alternative to metal machining to reduce the cost and weight of these components.

ACKNOWLEDGMENT

This research was supported by an appointment to the NASA Postdoctoral Program at the Jet Propulsion Laboratory, administered by Oak Ridge Associated Universities through a contract with NASA.

REFERENCES

[1] I. Gibson, D.W. Rosen, and B. Stucker, *Additive Manufacturing Technologies: Rapid Prototyping to Direct Digital Manufacturing*, New York: Springer, 2010.

[2] H. Lipson, and M. Kurman, *Fabricated: The New World of 3D Printing*, Hoboken, NJ: Wiley, 2013.

[3] E. Macdonald, R. Salas, D. Espalin, M. Perez, E. Aguilera, D. Muse, and R.B. Wicker, "3D printing for rapid prototyping of structural electronics," *IEEE Access,* vol.2, pp.234-242, Apr. 2014.

[4] G. Chattopadhyay, N. Llombart, C. Lee, C. Jung, R. Lin, K. B. Cooper, T.Reck, J.Siles, E.Schlecht, A.Peralta, B.Thomas, and I.Mehdi,"Terahertz array receivers with integrated antennas," inProc. IEEE Int.Workshop on Antenna Technol.(iWAT), Tucson, AZ, Mar. 2012.

[5] C.R. Garcia *et al.*, C.R., "Effects of extreme surface roughness on 3D printed horn antenna," *Electr. Lett.*, vol. 49, no. 12, pp. 734-736, June 2013.

[6] S. Groiss *et al.*, "Parameters of lossy cavity resonators calculated by the finite element method," IEEE Trans. Magn., vol. 32, no. 3, pp. 894-897, May 1996.

[7] I. Stil *et al.*, "Loss of WR10 Waveguide across 70-116 GHz," in *22nd International Symposium on Space Terahertz Technology*, Tokyo, 2012, pp. 151-153.

[8] A. R. Kerr *et al.*, "Loss of gold plated waveguides at 210-280 GHz," ALMA MEMO 585, 2009, pp. 1–6.

[9] E.O. Hammerstad, and F. Bekkadal, *A Microstrip Handbook, ELAB Report*, STF 44 A74169, University of Trondheim, Norway, 1975, pp 98-110.

[10] E. Decrossas**,** M.A. EL Sabbagh, V. Fouad Hanna and S.M. El-Ghazaly, "Mode Matching Technique Based Modeling of Coaxial and Circular Waveguide Discontinuities for Materials Characterization Purposes," *Int. J. Microw. Wireless Technologies,* vol. 3, pp. 679-690, Sept. 2011.

[11] J-C Samuel, B. Dick, S. Loui, and J.D. Rockway, "Development of a Ku-band corrugated conical horn using 3-D print technology," *IEEE Antennas Wireless Propag. Lett.*, vol. 13,pp. 201-204, 2014.

[12] E. Decrossas, T. Reck, C. Lee, C. Jung-Kubiak, I. Mehdi and G. Chattopadhyay, "Development of W-band horn antennas using 3D printing technologies", *IEEE Antennas Propagation Society Inter. Symp. (APSURSI)*, Fajardo, Puerto Rico, June 2016.